Dalton Transactions

ROYAL SOCIETY OF CHEMISTRY

PAPER

View Article Online
View Journal | View Issue

Cite this: *Dalton Trans.*, 2025, **54**, 8183

Achieving balanced UV SHG responses, optical band gaps and birefringence in rare earth compounds $Ln(IO_3)(SO_4)\cdot 3H_2O$ (Ln = Y, Gd, Er, Ho, Dy, Eu)†

Shihua Ma,[a] Lei Geng, *[a] Baozhu Zhu[a] and Changyu Meng*[b]

Received 14th March 2025,
Accepted 14th April 2025

DOI: 10.1039/d5dt00613a

rsc.li/dalton

A series of rare earth iodate sulfate UV compounds, $Ln(IO_3)(SO_4)\cdot 3H_2O$ (Ln = Y, Gd, Er, Ho, Dy, Eu), have been successfully synthesized by the hydrothermal method at 200 °C. These isostructural compounds all crystallize in the noncentrosymmetric space group $P2_12_12_1$ (no. 19) and feature a neutral three-dimensional $Ln(IO_3)(SO_4)$ framework which is composed of 2D cationic $Ln[SO_4]^+$ layers bridged by anionic $[IO_3]^-$ trigonal pyramids through sharing corner oxygen atoms. Under 1064 nm laser irradiation, $Y(IO_3)(SO_4)\cdot 3H_2O$ exhibits a second-harmonic generation (SHG) with an efficiency of 0.7 × KDP@1064 nm. Furthermore, $Y(IO_3)(SO_4)\cdot 3H_2O$ has a moderate birefringence (0.118@532 nm) and a large band gap (4.60 eV) and may be a potential UV nonlinear optical material. For $Eu(IO_3)(SO_4)\cdot 3H_2O$, it emits intense photoluminescence peaks at 594 nm and 617 nm when excited under 393 nm near-ultraviolet light, showing promising applications as red phosphors of white-LEDs. The current study elucidates that the incorporation of highly anisotropic lone-paired $(IO_3)^-$ units into highly isotropic $(SO_4)^{2-}$ sulfate groups can achieve balanced SHG responses, optical band gaps and birefringence, facilitating the development of novel iodate sulfate crystals for UV nonlinear optical applications.

Introduction

Rare earth compounds have multifunctional applications in luminescence, ceramic materials, catalysts, nonlinear laser crystals, *etc.*[1–5] From an atomic viewpoint, rare earth elements have fully occupied outermost and second outermost layers filled with electrons, and empty or singly occupied 5d orbitals, and the internal 4f orbitals have an increasing number of electrons as the atomic number increases. Additionally, rare earth elements exhibit flexible coordination capabilities, enabling them to combine with oxygen atoms to form various polyhedral LnO_x compounds (x = 6–10). These structures often exhibit distortions or noncentrosymmetric arrangements, which are highly advantageous for the formation of nonlinear optical crystals.[6–10] The recently synthesized noncentrosymmetric rare earth compounds, such as REI_5O_{14} (RE = Y and Gd) (14 × and 15 × KDP), $Cs_2YB_3O_6F_2$ (5.6 × KDP), and $Y_3F(SeO_3)_4$ (5.5 × KDP), exhibit strong second-harmonic generation (SHG) efficiency, making them promising candidates for nonlinear optical materials.[11–13] Several strategies have been employed to synthesize compounds with noncentrosymmetric structures. These include the introduction of second-order Jahn–Teller (SOJT) distortion d^0 transition metal (TM) cations (Mo^{6+}, V^{5+}, Nb^{5+}, Ti^{4+}, *etc.*), as seen in $K_3Nb_3Ge_2O_{13}$ and Li_2TiTeO_6;[14,15] the use of stereochemically active lone-pair (SCALP) cations (Bi^{3+}, Pb^{2+}, *etc.*), as in $BiO(IO_3)$ and $Cs_2Bi_2O(Ge_2O_7)$;[16,17] the incorporation of strongly electronegative F^- anions, as in $CaCe(IO_3)_3(IO_3F)F$ and $[GaF(H_2O)][IO_3F]$;[18,19] and the mixing of different types of anionic groups, as in $Cd_2(IO_3)(PO_4)$ and $AgBi(SO_4)(IO_3)_2$.[20,21]

I^{5+} ions may exhibit significant optical anisotropy due to the presence of lone-pair electrons, which strongly influence the SHG and birefringence properties of crystals. Sulfates and phosphates typically exhibit shorter UV absorption edges, which are significantly favorable for achieving large band gaps in compounds.[22–24] In rare earth iodate sulfates, due to the rich coordination environment of rare earth elements, many structures have been found such as $Ln(IO_3)(SO_4)$ (Ln = La–Gd, except Pm), $Ln_2(IO_3)_3(SO_4)OH\cdot 3H_2O$ (Ln = Sm, Eu, Dy), and $Ce(IO_3)_2(SO_4)$.[25–27] In several previous studies, heterovalent

[a]*School of Physics and Physical Engineering, Qufu Normal University, Qufu 273165, China. E-mail: lgeng@qfnu.edu.cn*
[b]*Guangxi Key Laboratory of Agricultural Resources Chemistry and Biotechnology, Department of Chemistry and Food Science, Yulin Normal University, Yulin 537000, China. E-mail: mengchyu_2007@163.com*

†Electronic supplementary information (ESI) available: Synthesis, property characterization and crystallographic data. CCDC 2431211-2431216. For ESI and crystallographic data in CIF or other electronic format see DOI: https://doi.org/10.1039/d5dt00613a

substitution has been recognized as an efficient way to synthesize non-centrosymmetric structures, for instance, from $Pb_2TiOF(SeO_3)_2Cl$ to $Pb_2GaF_2(SeO_3)_2Cl$,[28,29] from $CeF_2(SO_4)\cdot H_2O$ to $Ce(IO_3)_2(SO_4)$,[27] and from α- and β-$Ba_2[VO_2F_2(IO_3)_2](IO_3)$ to α- and β-$Ba_2[GaF_4(IO_3)_2](IO_3)$.[30,31] Building on the known crystal structures based on the above strategy, we experimentally introduced lone-paired [IO_3^-] groups into rare earth sulfates *via* the hydrothermal method, and successfully synthesized a new series of rare earth iodate sulfate compounds $Ln(IO_3)(SO_4)\cdot 3H_2O$ (Ln = Y, Gd, Er, Ho, Dy, Eu) with noncentrosymmetric structures and large UV absorption edges. Among these structures, $Y(IO_3)(SO_4)\cdot 3H_2O$ exhibits a wide band gap of 4.6 eV, a large SHG efficiency of 0.7 × KDP@1064 nm, and type-I phase matching, fully achieving balanced UV SHG efficiency and birefringence. In this study, the synthesis, crystal structures, infrared and UV–vis–NIR spectra, and fluorescence spectra of $Ln(IO_3)(SO_4)\cdot 3H_2O$ will be reported and discussed. This study demonstrates that combining large anisotropic [IO_3^-] groups with isotropic sulfates is an effective strategy for achieving a balance between UV SHG efficiency and birefringence properties.

Results and discussion

Crystal structure

Crystallographic data and refinement results are summarized in Table S1,† while atomic coordinates and bond valence sums (BVS) are provided in Table S2.† Selected bond lengths and bond angles are listed in Table S3.† The phase purity of the synthesized materials $Ln(IO_3)(SO_4)\cdot 3H_2O$ (Ln = Y, Gd, Er, Ho, Dy, Eu) was confirmed by XRD data comparison (Fig. S1†). EDS results show that the crystals contain elements and proportions consistent with the chemical formula (Fig. S2†). The crystal structures of the six crystals are isostructural, exemplified here by $Y(IO_3)(SO_4)\cdot 3H_2O$, which crystallizes in the non-centrosymmetric space group $P2_12_12_1$ (19). The asymmetric unit of $Y(IO_3)(SO_4)\cdot 3H_2O$ consists of one Y atom, one I atom, one S atom, ten oxygen atoms, and six hydrogen atoms. The I^{5+} cation is connected to three oxygens atoms, forming a distorted trigonal pyramid with bond lengths from 1.787(4) to 1.804(4) Å (Fig. 1a). The S^{6+} cation is connected to four oxygen atoms to form a [SO_4] tetrahedron with bond lengths from 1.449(4) to 1.485(4) Å. The Y^{3+} cation is coordinated by eight oxygen atoms to form the [YO_8] polyhedron with Y–O bond lengths from 2.262(4) to 2.450(4) Å. The overall structure is composed of three structural units, *i.e.*, [IO_3], [SO_4], and [YO_8], with each [YO_8] polyhedron linked to three [IO_3] trigonal pyramids, three [SO_4] tetrahedra, and two H_2O through sharing corner oxygen atoms with the monodentate method (Fig. 1b). It is observed along the *a*-axis that free water molecules are trapped in the cavity structure formed by four [YO_8], two [IO_3], and two [SO_4] units. The calculated BVS of Y, I, and S in $Y(IO_3)(SO_4)\cdot 3H_2O$ are +3.337, +5.268, and +6.095, respectively, closely matching their formal values and confirming the structural rationality of $Y(IO_3)(SO_4)\cdot 3H_2O$. The local dipole moments were calculated to analyze the geometric distortion of [IO_3], [SO_4], and [LnO_8] units for compounds $Ln(IO_3)(SO_4)\cdot 3H_2O$ (Ln = Y, Gd, Eu) (Table S4†). For $Y(IO_3)(SO_4)\cdot 3H_2O$, the calculated dipole moments of [IO_3], [SO_4], and [YO_8] units are 27.8823 D, 1.1702 D, and 4.3600 D, respectively. For $Gd(IO_3)(SO_4)\cdot 3H_2O$, the dipole moments of [IO_3], [SO_4], and [GdO_8] units are 27.8973 D, 1.1840 D, and 3.6735 D, respectively. For $Eu(IO_3)(SO_4)\cdot 3H_2O$, the dipole moments of the [IO_3], [SO_4] and [EuO_8] units are 27.7063 D, 1.2442 D, and 4.7849 D, respectively. Clearly, the distortions of the trigonal pyramidal [IO_3] and tetrahedral [SO_4] units are similar in these compounds, while the distortions of the [LnO_8] units follow the trend [EuO_8] > [YO_8] > [LnO_8], consistent with the SHG efficiency measurements.

From a structural evolution perspective, rare earth sulfates $Y(IO_3)(SO_4)\cdot 3H_2O$ can be considered derivatives formed by introducing an [IO_3] group into the parent structure of $Y_2(SO_4)_3\cdot 8H_2O$.[32] As is evident from Fig. 2, $Y_2(SO_4)_3\cdot 8H_2O$ has a two-dimensional neutral layer structure consisting of [YO_8] and [IO_3] functional units as well as crystal water. There are

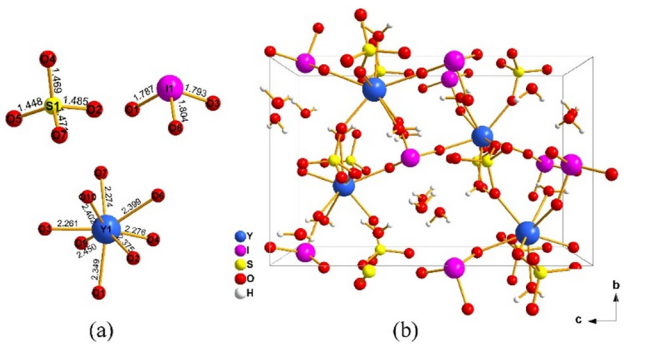

Fig. 1 The coordination environment of [SO_4], [IO_3], and [YO_8] units (a) and the crystal structure of $Y(IO_3)(SO_4)\cdot 3H_2O$ viewed down the *a*-axis (b).

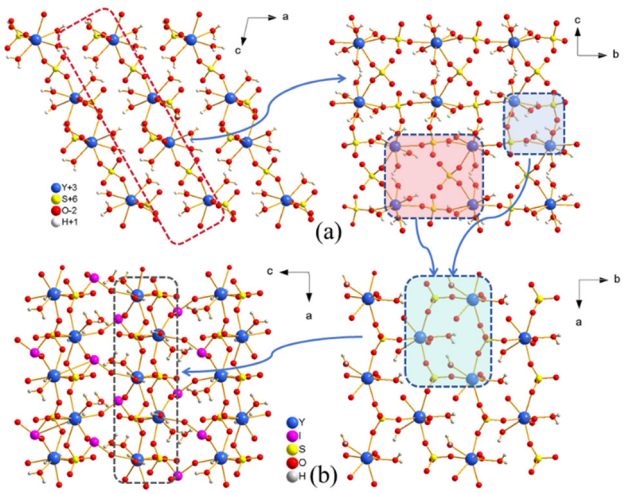

Fig. 2 Crystal structure comparison of $Y_2(SO_4)_3\cdot 8H_2O$ (a) and $Y(IO_3)(SO_4)\cdot 3H_2O$ (b).

two types of macrocyclic components in the two-dimensional layer of $Y_2(SO_4)_3{\cdot}8H_2O$ including a larger eight-membered ring composed of four [SO_4] tetrahedra and four [YO_8] polyhedra and a smaller four-membered ring composed of two [SO_4] tetrahedra and two [YO_8] polyhedral alternatively arranged along the *a*-axis direction. However, for the title compound $Y(IO_3)(SO_4){\cdot}3H_2O$, with the participation of [IO_3], the two kinds of macrocyclic Y–S–O rings converge into only one kind of six-membered ring, consisting of three [SO_4] tetrahedra and three [YO_8] polyhedra. The [IO_3] trigonal pyramids further bridge the adjacent two-dimensional $Y(SO_4)$ layers into a three-dimensional framework of $Y(IO_3)(SO_4){\cdot}3H_2O$. It is noteworthy that the introduction of [IO_3] into $Y_2(SO_4)_3{\cdot}8H_2O$ not only increases the dimensionality of the crystal structure but also facilitates the structural conversion from centrosymmetric to noncentrosymmetric space groups.

Infrared and UV–vis–NIR spectra

The infrared spectra of $Ln(IO_3)(SO_4){\cdot}3H_2O$ (Ln = Y, Gd, Er, Ho, Dy, Eu) are presented in Fig. S3.† All compounds have six characteristic absorption bands observed around 3300–3600, 1620–1650, 1100–900, 870–770, 660–500, and 500–400 cm^{-1}, showing a variety of symmetric and antisymmetric vibrations of O–H, S–O, and I–O bonds. Two absorption bands in the ranges of 3300–3600 and 1620–1650 cm^{-1} are attributed to the O–H bonds from hydroxyl groups, indicating the presence of crystal water molecules in the crystals. The absorption band at 1100–900 cm^{-1} is assigned to the symmetric stretching ν_1 modes of [SO_4]. The absorption spectrum in the range of 870–770 cm^{-1} can be attributed to the antisymmetric stretching ν_3 mode of [IO_3]. The range of 660–500 cm^{-1} is attributed to the antisymmetric bending ν_4 mode of [SO_4], and the absorption spectra in the range of 500–400 cm^{-1} can be attributed to the combined action of [IO_3^-] and [SO_4]. These assignments are consistent with previous literature.[33]

The UV–vis–NIR diffuse reflectance spectra of $Ln(IO_3)(SO_4){\cdot}3H_2O$ (Ln = Er, Ho, Dy, Eu) display characteristic electronic excitation, which is assigned and labeled in their respective spectra (Fig. S4†).[34–36] The band gaps of $Ln(IO_3)(SO_4){\cdot}3H_2O$ (Ln = Er, Ho, Dy, Eu) were determined to be 4.51 eV (Dy), 4.51 eV (Er), 4.52 eV (Ho), and 4.42 eV (Eu) by making tangent lines at the absorption edges (Fig. S5†). As shown in Fig. 3, the band gaps of $Y(IO_3)(SO_4){\cdot}3H_2O$ and $Gd(IO_3)(SO_4){\cdot}3H_2O$ are 4.6 eV and 4.55 eV, respectively. These values are higher than those of most iodate-based materials, such as $Bi_2O(SO_4)(IO_3)_2$ (2.40 eV),[37] $KBi(IO_3)_3(OH)$ (3.5 eV),[38] $KBi(SeO_4)(IO_3)Cl$ (3.9 eV),[39] and $Bi(IO_3)(SO_4)$ (3.91 eV).[33] This demonstrates that $Y(IO_3)(SO_4){\cdot}3H_2O$ and $Gd(IO_3)(SO_4){\cdot}3H_2O$ are promising candidates for UV optical materials.

Fluorescence

Due to the imperative necessity of f-block cations in the field of photoluminescence, we investigated the excitation and emission spectra of the compounds $Ln(IO_3)(SO_4){\cdot}3H_2O$ (Ln = Eu, Dy, Ho, Er) (Fig. 4). Under 393 nm near-ultraviolet excitation, $Eu(IO_3)(SO_4){\cdot}3H_2O$ exhibits two emission peaks: the strongest at 594 nm

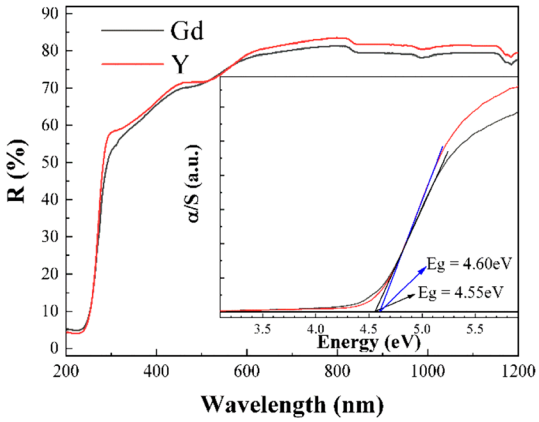

Fig. 3 UV–Vis–NIR diffuse reflectance spectra for $Gd(IO_3)(SO_4){\cdot}3H_2O$ and $Y(IO_3)(SO_4){\cdot}3H_2O$.

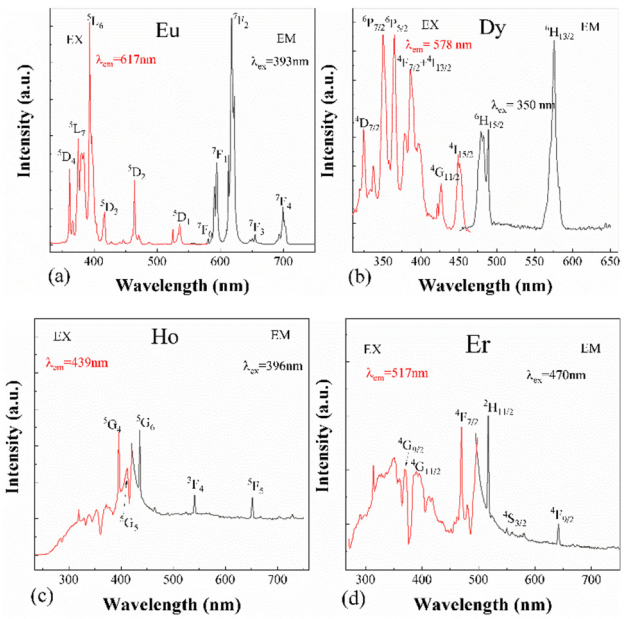

Fig. 4 Excitation and emission spectra for $Ln(IO_3)(SO_4){\cdot}3H_2O$ (Ln = Eu (a), Dy (b), Ho (c), Er (d)).

and the next strongest at 617 nm, corresponding to the $^5D_0 \rightarrow {}^7F_1$ and $^5D_0 \rightarrow {}^7F_2$ transitions of Eu^{3+} ions, respectively (Fig. 4a).[40] The excitation spectrum of $Dy(IO_3)(SO_4){\cdot}3H_2O$ displays multiple absorption peaks at 324 nm ($^6P_{3/2}$), 350 nm ($^6P_{7/2}$), 365 nm ($^6P_{7/2}$), 386 nm ($^4F_{7/2} + {}^4I_{13/2}$), and 449 nm ($^4I_{15/2}$) when the emission is monitored at 578 nm. However, under 350 nm excitation, only two main emission bands are observed: the strongest emission peak at 578 nm ($^4F_{7/2} \rightarrow {}^6H_{13/2}$) and a secondary emission peak at 490 nm ($^4F_{9/2} \rightarrow {}^6H_{15/2}$) (Fig. 4b). In the case of Ho^{3+} ions in $Ho(IO_3)(SO_4){\cdot}3H_2O$, a strong and narrow emission peak at 396 nm is observed when monitored at 439 nm emission wavelength (Fig. 4c).[41] Similarly, under 470 nm near-ultraviolet excitation, the Er^{3+} ions in $Er(IO_3)(SO_4){\cdot}3H_2O$ exhibit a strong and narrow emission peak at 517 nm (Fig. 4d).[42,43]

SHG properties

The SHG responses of the six crystals were measured under 1064 nm radiation using the conventional Kurtz–Perry method. As shown in Fig. 5 and Fig. S6,† although all six crystals crystallize in noncentrosymmetric space groups, the SHG effect for Er$(IO_3)(SO_4)\cdot 3H_2O$, Dy$(IO_3)(SO_4)\cdot 3H_2O$, and Ho$(IO_3)(SO_4)\cdot 3H_2O$ is too weak to be measured. In contrast, Y$(IO_3)(SO_4)\cdot 3H_2O$ and Gd$(IO_3)(SO_4)\cdot 3H_2O$ exhibit their largest SHG effect at particle sizes of 100–150 μm, with SHG intensities of 0.7 × KDP and 0.9 × KDP, respectively. Meanwhile, Eu$(IO_3)(SO_4)\cdot 3H_2O$ reaches its maximum SHG intensity of about 1.1 × KDP at particle sizes of 180–250 μm. However, neither Gd$(IO_3)(SO_4)\cdot 3H_2O$ nor Eu$(IO_3)(SO_4)\cdot 3H_2O$ can achieve phase matching, as indicated by the trend of SHG intensities *versus* particle sizes. The SHG intensities of Y$(IO_3)(SO_4)\cdot 3H_2O$ increase with the increase of particle sizes and substantially remain unchanged at larger size ranges, suggesting the phase-matching ability of the crystal. Calculations of dipole moments reveal that the $[IO_3]$ group makes a prominent contribution to the SHG response of the crystals. The calculated dipole moment of the $[EuO_8]$ polyhedron is 4.7849 D, largest among the three crystals (Ln = Y, Gd, Eu) and the experimentally determined SHG intensity of Eu$(IO_3)(SO_4)\cdot 3H_2O$ is also the highest. These results highlight the significant contribution of the $[LnO_8]$ polyhedra to the SHG responses in the Ln$(IO_3)(SO_4)\cdot 3H_2O$ (Ln = Y, Gd, Eu) systems, which should not be overlooked. Given that the SHG effect and band gap are two critical optical parameters for evaluating nonlinear optical materials, we compared the SHG responses and band gaps of Y$(IO_3)(SO_4)\cdot 3H_2O$ and Gd$(IO_3)(SO_4)\cdot 3H_2O$ with some selected iodate sulfate crystals (Table 1).

Theoretical analysis

To understand the microscopic mechanisms underlying the optical properties of Y$(IO_3)(SO_4)\cdot 3H_2O$, theoretical calculations have been carried out using the first principles method within the framework of plane-wave-based pseudopotential density-functional theory (DFT). The calculated band structure of compound Y$(IO_3)(SO_4)\cdot 3H_2O$ in Fig. 6a reveals an indirect band gap of 4.034 eV, which is slightly lower than the experimental value of 4.60 eV obtained from UV–vis–NIR diffuse reflectance spectra. This discrepancy arises from the shortcoming of the conventional DFT-GGA-PBE functional, which tends to lower the conduction band energy levels, leading to an underestimation of the calculated band gap.[49–52] From the total density of states (TDOS) and partial density of states (PDOS) of Y$(IO_3)(SO_4)\cdot 3H_2O$, it is evident that the top of the valence band (VB) is primarily contributed by the I-5s5p and O-2p orbitals. In contrast, the bottom of the conduction band (CB) is mainly contributed by the I-5p, O-2p, and Y-4d orbitals (Fig. 6b). Since the optical properties depend closely on the electron transitions from the VB to the CB, the results of theoretical analysis suggest that the synergistic interaction between the $[YO_8]$ polyhedra and $[IO_3]$ trigonal pyramids is the primary origin of the optical absorption in Y$(IO_3)(SO_4)\cdot 3H_2O$.

The birefringence of Y$(IO_3)(SO_4)\cdot 3H_2O$ is significantly enhanced by the introduction of highly anisotropic $[IO_3]$ units. For comparison, the calculated birefringence of $Y_2(SO_4)_3\cdot 8H_2O$ is only 0.004 @ 532 nm, whereas the refractive index of Y$(IO_3)(SO_4)\cdot 3H_2O$ is calculated to be 0.118 @ 532 nm (Fig. 7). Furthermore, the birefringence of Y$(IO_3)(SO_4)\cdot 3H_2O$ exceeds those of most metal sulfate materials, such as $RbY(SO_4)_2\cdot 4H_2O$ (0.045 @ 546 nm),[53] $Hg_3O_2SO_4$ (0.100 @ 546 nm),[54] and

Table 1 Comparison of the space groups, SHG, and band gaps of iodate or sulfate anionic groups

Crystal	Space group	SHG response (×KDP)	Band gaps (eV)
$Bi_2O(SO_4)(IO_3)_2$ [37]	$P21/n$	0	2.40
$Ba_2Ce(IO_3)_8(H_2O)$ [44]	$Pna2_1$	0.2	2.44
$BaZr(IO_3)_6$ [45]	$P\bar{1}$	0	3.1
$KBi(IO_3)_3(OH)$ [38]	$P\bar{1}$	0	3.5
$Bi(IO_3)(SO_4)$ [33]	$P2_1/c$	0	3.91
$CdBi(IO_3)(SO_4)_2$ [33]	$P2_1/c$	0	4.03
$Rb_2SO_4\cdot SbF_3$ [46]	$P2_12_12_1$	0.3	4.15
$NaGaI_3O_9F$ [47]	$P2_1/c$	0	4.27
$K_2SO_4\cdot SbF_3$ [46]	$P2_12_12_1$	0.1	4.44
$Na_7(IO_3)(SO_4)_3$ [48]	$P2_12_12_1$	0.5	4.83
$Gd(IO_3)(SO_4)\cdot 3H_2O$	$P2_12_12_1$	0.8	4.55
$Y(IO_3)(SO_4)\cdot 3H_2O$	$P2_12_12_1$	0.7	4.6

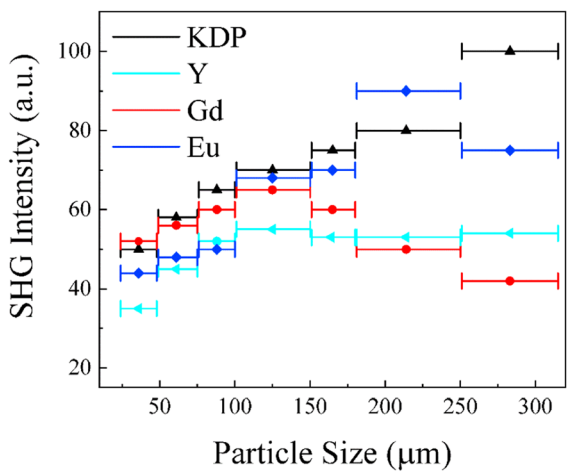

Fig. 5 SHG intensity for samples Ln$(IO_3)(SO_4)\cdot 3H_2O$ (Ln = Y, Gd and Eu) and standard KDP with different particle sizes.

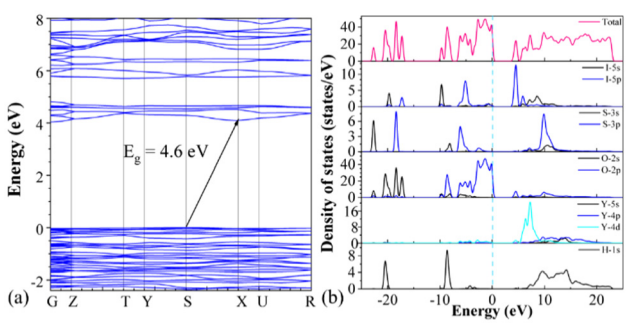

Fig. 6 Calculated band structure (a) and DOS (b) of Y$(IO_3)(SO_4)\cdot 3H_2O$.

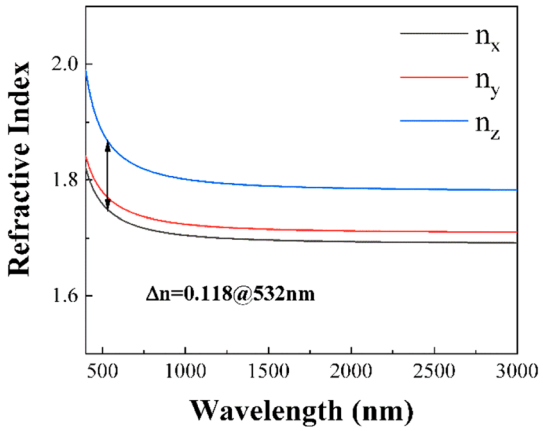

Fig. 7 Calculated refractive index for $Y(IO_3)(SO_4)\cdot 3H_2O$ crystals.

$RbSbSO_4Cl_2$ (0.110 @ 1064 nm).[55] The sufficiently large birefringence of 0.118 at 532 nm for $Y(IO_3)(SO_4)\cdot 3H_2O$ explains its phase-matchable SHG responses.

Conclusions

In summary, we successfully synthesized a series of rare earth iodate sulfates $Ln(IO_3)(SO_4)\cdot 3H_2O$ (Ln = Y, Gd, Er, Ho, Dy, Eu) with noncentrosymmetric structures. Among these, $Eu(IO_3)(SO_4)\cdot 3H_2O$ exhibits a large SHG response of 1.1 × KDP at particle sizes of 180–250 μm, while $Gd(IO_3)(SO_4)\cdot 3H_2O$ and $Y(IO_3)(SO_4)\cdot 3H_2O$ show SHG responses of 0.9 × and 0.7 × KDP at particle sizes of 100–150 μm, respectively. The three-in-one combination of rare earth, iodate, and sulfate functional units results in a comprehensive enhancement of both the SHG effect and optical band gap. The findings of this work provide a feasible design strategy for exploring new nonlinear optical materials that simultaneously exhibit large SHG responses and wide band gaps. Although the other three compounds, $Ln(IO_3)(SO_4)\cdot 3H_2O$ (Ln = Er, Ho, Dy), do not display SHG responses, they demonstrate interesting fluorescence properties and can serve as host crystals of rare earth dopants, making them promising candidates for next-generation lighting materials.

Data availability

Crystallographic data have been deposited at the CCDC with deposition numbers 2431211–2431216.† The data supporting this article have been included as part of the ESI,† including synthesis and property characterization; details of crystallographic refinement; atomic coordinates and BVS; bond lengths and angles; dipole moments; PXRD patterns; EDS; infrared spectroscopy; UV–vis–NIR diffuse reflectance; and SHG intensity.

Conflicts of interest

There are no conflicts to declare.

Acknowledgements

This research is supported by the Natural Science Foundation of Shandong Province (ZR2020ME021), the Program of High-level Talents Research Funding of Yulin Normal University (G2020ZK20 and G2020ZK21), and the Project of the Cultivation of Middle-aged and Young Backbone Teachers in Guangxi Colleges and Universities (1000 Plan).

References

1 E. E. Oyeka, M. J. Winiarski, H. Swiatek, W. Balliew, C. D. McMillen, M. L. Liang, M. I. Sorolla and T. T. Tran, $Ln_2(SeO_3)_2(SO_4)(H_2O)_2$ (Ln = Sm, Dy, Yb): A Mixed-Ligand Pathway to New Lanthanide(III) Multifunctional Materials Featuring Nonlinear Optical and Magnetic Anisotropy Properties, *Angew. Chem., Int. Ed.*, 2022, **61**, e202213499.
2 C. K. Aslani, V. V. Klepov, M. A. A. Aslani and H. C. Z. Loye, Hydrothermal Synthesis of New Iodates $Ln_2(IO_3)_3(IO_4)$ (Ln = La, Nd, Pr) Containing the Tetraoxoiodate(V) Anion: Creation of Luminescence Properties by Doping with Eu, Dy, and Tb, *Cryst. Growth Des.*, 2021, **21**, 4707–4712.
3 N. Haldar, T. Mondal, T. Das, D. Sarkar, M. Pal, A. H. Seikh and C. K. Ghosh, A truncated octahedron $NaCe(MoO_4)_2$ nanostructure: a potential material for blue emission and acetone sensing, *Mater. Adv.*, 2024, **5**, 4480–4490.
4 Y. Suffren, O. Leynaud, P. Plaindoux, A. Brenier and I. Gautier-Luneau, Differences and Similarities between Lanthanum and Rare-Earth Iodate Anhydrous Polymorphs: Structures, Thermal Behaviors, and Luminescent Properties, *Inorg. Chem.*, 2016, **55**, 11264–11272.
5 L. Geng, C. Y. Meng and Q. Yan, Polar lanthanide copper iodates $LnCu(IO_3)_5$ (Ln = La, Ce, Pr, and Nd): Synthesis, crystal structure and characterization, *J. Solid State Chem.*, 2022, **308**, 122934.
6 J. Song, C. G. Li, J. M. Jiao, Y. H. She, W. L. Zhao, F. Liang, N. Ye, Z. G. Hu and Y. C. Wu, $KNa_2La_2(BO_3)_3$: a shortite-type lanthanide borate exhibiting strong nonlinear optical activity induced by isolated $[BO_3]$ triangles and distorted $[LaO_9]$ polyhedra, *Inorg. Chem. Front.*, 2023, **10**, 5488–5495.
7 P. F. Li, C. L. Hu, B. X. Li, F. Kong and J. G. Mao, $Y(HSeO_3)(SeO_3)(H_2O)\cdot(H_2O)$ and $Y_2(SeO_3)_2(SeO_4)(H_2O)_2\cdot(H_2O)_{0.75}$: Two yttrium selenites with a short UV cut-off edge explored from pure selenite compounds, *J. Alloys Compd.*, 2023, **959**, 170570.
8 A. M. Li, D. K. Xu, H. Lin, S. H. Yang, Y. Z. Shao and Y. L. Zhang, $NaGd(MoO_4)_2$ nanocrystals with diverse morphologies: controlled synthesis, growth mechanism, photoluminescence and thermometric properties, *Sci. Rep.*, 2016, **6**, 31366.
9 Q. Wu, X. Liu, S. R. Xu, H. B. Pi and Y. J. Li, Five New Silver Rare–Earth Iodates, $AgLn(IO_3)_4$ (Ln = Pr, Sm, Dy, Er and Tm): Synthesis, Structures and Properties, *ChemistrySelect*, 2019, **4**, 8709–8712.

10 P. F. Li, C. L. Hu, J. G. Mao and F. Kong, A UV non-hydrogen pure selenite nonlinear optical material for achieving balanced properties through framework-optimized structural transformation, *Mater. Horiz.*, 2024, **11**, 1704–1709.
11 J. Chen, C. L. Hu, F. F. Mao, B. P. Yang, X. H. Zhang and J. G. Mao, REI_5O_{14} (RE = Y and Gd): Promising SHG Materials Featuring the Semicircle-Shaped $I_5O_{14}^{3-}$ Polyiodate Anion, *Angew. Chem., Int. Ed.*, 2019, **58**, 11666–11669.
12 H. P. Wu, Z. J. Wei, Z. G. Hu, J. Y. Wang, Y. C. Wu and H. W. Yu, Assembly of π-Conjugated $[B_3O_6]$ Units by Mer-Isomer $[YO_3F_3]$ Octahedra to Design a UV Nonlinear Optical Material, $Cs_2YB_3O_6F_2$, *Angew. Chem., Int. Ed.*, 2024, **63**, e202406318.
13 P. F. Li, C. L. Hu, F. Kong and J. G. Mao, The First UV Nonlinear Optical Selenite Material: Fluorination Control in $CaYF(SeO_3)_2$ and $Y_3F(SeO_3)_4$, *Angew. Chem., Int. Ed.*, 2023, **62**, e202301420.
14 C. Chen, J. Chen, G. Yang, H. Tian, M. Luo, T. Yan, Z. Hu, J. Wang, Y. Wu, N. Ye and G. Peng, Intense d-p Hybridization in Nb_3O_{15} Tripolymer Induced the Largest Second Harmonic Generation Response and Birefringence in Germanates, *Angew. Chem., Int. Ed.*, 2023, **62**, e202217039.
15 X. L. Du, X. J. Guo, Z. L. Gao, F. A. Liu, F. F. Guo, S. Y. Wang, H. Y. Wang, Y. X. Sun and X. T. Tao, Li_2MTeO_6(M = Ti, Sn): Mid-Infrared Nonlinear Optical Crystal with Strong Second Harmonic Generation Response and Wide Transparency Range, *Angew. Chem., Int. Ed.*, 2021, **60**, 23320–23326.
16 S. D. Nguyen, J. Yeon, S. H. Kim and P. S. Halasyamani, $BiO(IO_3)$: A New Polar iodate that Exhibits an Aurivillius-Type $(Bi_2O_2)^{2+}$ Layer and a Large SHG Response, *J. Am. Chem. Soc.*, 2011, **133**, 12422–12425.
17 R. L. Tang, C. L. Hu, B. L. Wu, Z. Fang, Y. Chen and J. G. Mao, $Cs_2Bi_2O(Ge_2O_7)$ (CBGO): A Larger SHG Effect Induced by Synergistic Polarizations of BiO_5 Polyhedra and GeO_4 Tetrahedra, *Angew. Chem., Int. Ed.*, 2019, **58**, 15358–15361.
18 N. Ma, C. L. Hu, J. Chen, Z. Fang, Y. Huang, B. X. Li and J. G. Mao, $CaCe(IO_3)_3(IO_3F)F$: a promising nonlinear optical material containing both IO_3^- and IO_3F^{2-} anions, *Inorg. Chem. Front.*, 2022, **9**, 5478–5485.
19 Q. M. Huang, C. L. Hu, B. P. Yang, Z. Fang, Y. Lin, J. Chen, B. X. Li and J. G. Mao, $[GaF(H_2O)][IO_3F]$: a promising NLO material obtained by anisotropic polycation substitution, *Chem. Sci.*, 2021, **12**, 9333–9338.
20 Q. Q. Chen, C. L. Hu, L. J. Yao, J. Chen, M. Y. Cao, B. X. Li and J. G. Mao, $Cd_2(IO_3)(PO_4)$ and $Cd_{1.62}Mg_{0.38}(IO_3)(PO_4)$: metal iodate-phosphates with large SHG responses and wide band gaps, *Chem. Commun.*, 2022, **58**, 7694–7697.
21 H. M. Liu, Q. C. Wu, L. L. Liu, Z. S. Lin, P. S. Halasyamani, X. G. Chen and J. G. Qin, $AgBi(SO_4)(IO_3)_2$: aliovalent substitution induces structure dimensional upgrade and second harmonic generation enhancement, *Chem. Commun.*, 2021, **57**, 3712–3715.
22 Y. Q. Li, F. Liang, S. G. Zhao, L. N. Li, Z. Y. Wu, Q. R. Ding, S. Liu, Z. S. Lin, M. C. Hong and J. H. Luo, Two Non-π-Conjugated Deep-UV Nonlinear Optical Sulfates, *J. Am. Chem. Soc.*, 2019, **141**, 3833–3837.
23 Y. Q. Li, S. G. Zhao, P. Shan, X. F. Li, Q. R. Ding, S. Liu, Z. Y. Wu, S. S. Wang, L. N. Li and J. H. Luo, $Li_8NaRb_3(SO_4)_6{\cdot}2H_2O$ as a new sulfate deep-ultraviolet nonlinear optical material, *J. Mater. Chem. C*, 2018, **6**, 12240–12244.
24 X. H. Dong, Y. Long, X. Y. Zhao, L. Huang, H. M. Zeng, Z. E. Lin, X. Wang and G. H. Zou, $A_6Sb_4F_{12}(SO_4)_3$ (A = Rb, Cs): Two Novel Antimony Fluoride Sulfates with Unique Crown-like Clusters, *Inorg. Chem.*, 2020, **59**, 8345–8352.
25 H. J. Lu, X. J. Guo, Y. X. Wang, K. Diefenbach, L. H. Chen, J. Q. Wang, J. Lin and S. A. Wang, Size-dependent selective crystallization using an inorganic mixed-oxoanion system for lanthanide separation, *Dalton Trans.*, 2019, **48**, 12808–12811.
26 C. K. Aslani, V. V. Klepov and H. C. zur Loye, Hydrothermal synthesis of new mixed-oxoanion materials: Rare earth iodate sulfates $Sm(IO_3)(SO_4)$ and $Ln_2(IO_3)_3(SO_4)OH{\cdot}3H_2O$ (Ln = Sm, Eu, Dy), *Solid State Sci.*, 2022, **129**, 106918.
27 T. H. Wu, X. X. Jiang, Y. R. Zhang, Z. J. Wang, H. Y. Sha, C. Wu, Z. S. Lin, Z. P. Huang, X. F. Long, M. G. Humphrey and C. Zhang, From $CeF_2(SO_4){\cdot}H_2O$ to $Ce(IO_3)_2(SO_4)$: Defluorinated Homovalent Substitution for Strong Second-Harmonic-Generation Effect and Sufficient Birefringence, *Chem. Mater.*, 2021, **33**, 9317–9325.
28 X. L. Cao, C. L. Hu, X. Xu, F. Kong and J. G. Mao, $Pb_2TiOF(SeO_3)_2Cl$ and $Pb_2NbO_2(SeO_3)_2Cl$: small changes in structure induced a very large SHG enhancement, *Chem. Commun.*, 2013, **49**, 9965–9967.
29 F. G. You, F. Liang, Q. Huang, Z. G. Hu, Y. C. Wu and Z. S. Lin, $Pb_2GaF_2(SeO_3)_2Cl$: Band Engineering Strategy by Aliovalent Substitution for Enlarging Bandgap while Keeping Strong Second Harmonic Generation Response, *J. Am. Chem. Soc.*, 2019, **141**, 748–752.
30 H. W. Yu, M. L. Nisbet and K. R. Poeppelmeier, Assisting the Effective Design of Polar Iodates with Early Transition-Metal Oxide Fluoride Anions, *J. Am. Chem. Soc.*, 2018, **140**, 8868–8876.
31 J. Chen, C. L. Hu, F. F. Mao, J. H. Feng and J. G. Mao, A Facile Route to Nonlinear Optical Materials: Three-Site Aliovalent Substitution Involving One Cation and Two Anions, *Angew. Chem., Int. Ed.*, 2019, **58**, 2098–2102.
32 P. Held and M. Wickleder, Yttrium(III) sulfate octahydrate, *Acta Crystallogr., Sect. E: Struct. Rep. Online*, 2003, **59**, i98–i100.
33 Y. L. Li, C. L. Hu, J. Chen and J. G. Mao, Two bismuth iodate sulfates with enhanced optical anisotropy, *Dalton Trans.*, 2021, **50**, 16139–16146.
34 W. T. Carnall, P. R. Fields and K. Rajnak, Spectral Intensities of the Trivalent Lanthanides and Actinides in Solution. II. Pm^{3+}, Sm^{3+}, Eu^{3+}, Gd^{3+}, Tb^{3+}, Dy^{3+}, and Ho^{3+}, *J. Chem. Phys.*, 1968, **49**, 4412–4423.
35 W. T. Carnall, P. R. Fields and K. Rajnak, Electronic Energy Levels of the Trivalent Lanthanide Aquo Ions. IV. Eu^{3+}, *J. Chem. Phys.*, 1968, **49**, 4450–4455.

36 M. Y. Qie, J. Lin, F. Kong, M. A. Silver, Z. H. Yue, X. M. Wang, L. J. Zhang, H. L. Bao, T. E. Albrecht-Schmitt and J. Q. Wang, A Large Family of Centrosymmetric and Chiral f-Element-Bearing Iodate Selenates Exhibiting Coordination Number and Dimensional Reductions, *Inorg. Chem.*, 2018, **57**, 1676–1683.

37 L. Shi, D. J. Mei, J. L. Xu and Y. D. Wu, $Bi_2O(XO_4)(IO_3)_2$ (X = S, Se, Cr): Three-dimensional frameworks containing $[Bi_4O_2]^{8+}$ clusters, *Solid State Sci.*, 2017, **63**, 54–61.

38 Y. J. Jia, Y. G. Chen, T. Wang, Y. Guo, X. F. Guan and X. M. Zhang, $KBi(IO_3)_3(OH)$ and $NaBi(IO_3)_4$: from the centrosymmetric chain to a noncentrosymmetric double layer, *Dalton Trans.*, 2019, **48**, 10320–10326.

39 L. Geng, S. H. Ma, B. Z. Zhu, W. F. Li, K. Y. Jiang, H. Y. Lu, Q. Yan and C. Y. Meng, $KBi(SeO_4)(IO_3)Cl$: A mixed-anion oxychloride with three types of building units in one structure, *J. Solid State Chem.*, 2024, **329**, 124385.

40 A. S. Souza, Y. A. R. Oliveira and M. A. Couto dos Santos, Enhanced approach to the Eu^{3+} ion $^5D_0 \rightarrow {}^7F_0$ transition intensity, *Opt. Mater.*, 2013, **35**, 1633–1635.

41 Z. G. Feng, H. P. Xia, C. Wang, Z. X. Zhang, D. S. Jiang, J. Zhang, S. N. He, Q. Y. Tang, Q. G. Sheng, X. M. Gu, Y. P. Zhang, B. J. Chen and H. C. Jiang, Fluorescence spectra of $Na_5Lu_9F_{32}$ single crystals co-doped with Ho^{3+}/Tm^{3+} grown by Bridgman method, *Chem. Phys. Lett.*, 2016, **652**, 68–72.

42 J. A. Sanz-García, G. Lifante-Pedrola, J. E. M. Santiuste and E. Cantelar, Dual luminescent nano-thermometry based on the selective excitation of optical centers in $CaF_2:Er^{3+}$ nanoparticles, *J. Alloys Compd.*, 2025, **1010**, 177529.

43 C. Tian, J. Ruan, X. J. Zhao, J. J. Han and C. Liu, Structure, spectroscopic properties and optical temperature-sensing behavior of glass-ceramics containing polymorphic $CaTa_2O_6:Er^{3+}/Yb^{3+}$ nanocrystals, *J. Mater. Chem. C*, 2024, **12**, 16594–16607.

44 X. Y. Zhang, X. H. Zhang, B. P. Yang and J. G. Mao, A new polar alkaline earth-rare earth iodate: $Ba_2Ce(IO_3)_8(H_2O)$, *Dalton Trans.*, 2023, **52**, 4423–4428.

45 H. S. Ahn, D. W. Lee and K. M. Ok, Dimensionality variations in new zirconium iodates: hydrothermal syntheses, structural determination, and characterization of $BaZr(IO_3)_6$ and $K_2Zr(IO_3)_6$, *Dalton Trans.*, 2014, **43**, 10456–10461.

46 F. F. He, L. Wang, C. F. Hu, J. Zhou, Q. Li, L. Huang, D. J. Gao, J. Bi, X. Wang and G. H. Zou, Cation-tuned synthesis of the $A_2SO_4.SbF_3$ (A = Na^+, NH_4^+, K^+, Rb^+) family with nonlinear optical properties, *Dalton Trans.*, 2018, **47**, 17486–17492.

47 D. D. Wang, P. F. Gong, X. Y. Zhang, Z. S. Lin, Z. G. Hu and Y. C. Wu, $NaGaI_3O_9F$: a new alkali metal gallium iodate combined with IO_3^- and $IO_3F_2^-$ units, *Dalton Trans.*, 2021, **50**, 11562–11567.

48 M. M. Ding, H. W. Yu, Z. G. Hu, J. Y. Wang and Y. C. Wu, $Na_7(IO_3)(SO_4)_3$: the first noncentrosymmetric alkaline-metal iodate-sulfate with isolated $[IO_3]$ and $[SO_4]$ units, *Chem. Commun.*, 2021, **57**, 9598–9601.

49 Q. Q. Chen, C. L. Hu, B. X. Li and J. G. Mao, $[M(OH)_2]_3(IO_3)(SeO_4)\cdot H_2O$ (M = Ga and In): metal iodate–selenate nonlinear optical materials with a hexagonal tungsten oxide-type topology, *Inorg. Chem. Front.*, 2023, **10**, 3121–3130.

50 L. Geng, C. Y. Meng, H. Y. Lu, Z. Z. Luo, C. S. Lin and W. D. Cheng, $Bi_2Te(IO_3)O_5Cl$: a novel polar iodate oxychloride exhibiting a second-order nonlinear optical response, *Dalton Trans.*, 2015, **44**, 2469–2475.

51 Q. Li, H. N. Liu, H. W. Yu, Z. G. Hu, J. Y. Wang, Y. C. Wu and H. P. Wu, Alignment of Λ-Shaped Basic Building Units to Construct One New $KMoO_3(IO_3)$ Polar Polymorph, *Inorg. Chem.*, 2023, **62**, 3896–3903.

52 C. Y. Meng, L. Geng, W. T. Chen, M. F. Wei, K. Dai, H. Y. Lu and W. D. Cheng, Syntheses, structures, and characterizations of a new second-order nonlinear optical material: $Pb_2(SeO_3)(NO_3)_2$, *J. Alloys Compd.*, 2015, **640**, 39–44.

53 W. Lu, Y. Shen and Q. Wu, $RbY(SO_4)_2\cdot 4H_2O$: A new ultraviolet birefringent crystal, *J. Solid State Chem.*, 2024, **333**, 124546.

54 X. Dong, L. Huang, H. Zeng, Z. Lin, K. M. Ok and G. Zou, High-Performance Sulfate Optical Materials Exhibiting Giant Second Harmonic Generation and Large Birefringence, *Angew. Chem., Int. Ed.*, 2022, **61**, e202116790.

55 F. He, Y. Deng, X. Zhao, L. Huang, D. Gao, J. Bi, X. Wang and G. Zou, $RbSbSO_4Cl_2$: an excellent sulfate nonlinear optical material generated due to the synergistic effect of three asymmetric chromophores, *J. Mater. Chem. C*, 2019, **7**, 5748–5754.